Flux calibration of point and extended sources in the *AKARI* far-IR all-sky survey maps[*]

Toshiya Ueta,[1] Ryszard Szcerba,[2] Andrew Fullard,[1] and Satoshi Takita[3]

[1]*Department of Physics and Astronomy, University of Denver, Denver, CO 80208, USA*

[2]*Nicolaus Copernicus Astronomical Centre, PAS, ul. Rabiańska 8, 87-100 Toruń, Poland*

[3]*Institute of Space and Astronautical Science, Japan Aerospace Exploration Agency, 3-1-1 Yoshinodai, Chuo, Sagamihara, Kanagawa 252-5210, Japan*

ABSTRACT

The *AKARI* Infrared Astronomical Satellite produced the far-IR all-sky survey (AFASS) maps at roughly arc-minute spatial resolution with its Far-IR Surveyor (FIS) instrument. The AFASS maps enable us to probe the whole sky for sources having far-IR surface brightnesses higher than a few to a couple of dozen MJy sr^{-1}. While the AFASS maps are absolutely calibrated against large-scale diffuse background emission, it is uncertain whether or not an additional flux correction is necessary for small-scale compact and point sources. Here, we verify that point-source photometry reproduces fluxes in the *AKARI*-FIS bright source catalogue (BSC) as long as the aperture correction based on the empirical point-spread-function profiles of the AFASS maps is applied. This means that far-IR photometry of any source can be done from the AFASS maps by summing surface brightness pixel values within an appropriately-defined perimeter of the target source.

Keywords: infrared: general, methods: data analysis, techniques: image processing, techniques: photometric

1. INTRODUCTION

The Far-Infrared Surveyor (FIS: Kawada et al. 2007) is one of the two instruments aboard the *AKARI* infrared astronomical satellite (*AKARI*; Murakami et al. 2007), covering from 50 to 110 μm and 110 to 180 μm with two sets of Ge:Ga arrays, the Short Wavelength (SW) and Long Wavelength (LW) detectors, respectively. *AKARI* swept more than 98% of the entire sky at 3.′6 s^{-1} during all-sky survey observations (Doi et al. 2015). The absolute surface brightness calibration of FIS was done through (1) pre-launch measurements of a blackbody source which indicated a 5% accuracy, and (2) in-orbit comparisons between FIS and COBE/DIRBE measurements of infrared cirrus (Matsuura et al. 2011).

The additional absolute calibration of the resulting *AKARI* far-infrared all-sky survey (AFASS) maps[1] was done via iterative comparisons between the surface brightnesses in the AFASS images and expected surface brightnesses based on the DIRBE zodi-subtracted mission-average data (Hauser et al. 1998) augmented by the Gorjian zodi-model (Gorjian et al. 2000). Uncertainties in the archived AFASS maps were determined to be less than 10% for surface brightnesses of diffuse background emission greater than 10, 3, 25, and 26 MJy sr^{-1} at the *N60*, *WIDE-S*, *WIDE-L*, and *N160* bands, respectively, at the spatial resolution of DIRBE at approximately half a degree (Boggess et al. 1992; Takita et al. 2015).

However, when aperture photometry with a fixed 90″ radius aperture and the 120–300″ radius sky annulus was performed for a set of Cohen infrared standard stars (Cohen et al. 1999) detected in the AFASS maps in the *N60*, *WIDE-S*, and *WIDE-L* bands, the resulting fluxes came out to be roughly 30–60% less than expected (Arimatsu et al. 2014). The observed flux underestimates of Cohen calibrators in the AFASS maps were attributed to the unobserved extended PSF component beyond the 90″ radius aperture, because (1) the slow transient effects of the FIS detector seen in the slow-scan mode at 8 or 15″ s^{-1} (Shirahata et al. 2009; Ueta et al. 2017) are far less likely to occur in the all-sky survey mode at 3.′6 s^{-1}, and (2) the flux-dependent detector response was not confirmed in the AFASS maps (Takita et al. 2015).

Because many Cohen standards in the previous analysis (0.02–10 Jy; Arimatsu et al. 2014) fell outside of *AKARI*'s detection limit, a stacking method had to be used to improve on the signal-to-noise ratio (S/N) of the data. Thus, in the present work, we aim to verify if the missed extended component of the PSF is truly the cause of the observed flux underestimates by performing photometry with bright point sources listed in the *AKARI*/FIS Bright source catalogue (BSC) in all four bands via the PSF aperture photometry with an aperture correction and contour photometry.

Corresponding author: Toshiya Ueta

toshiya.ueta@du.edu

2. ESTABLISHING THE PSF IN THE AFASS IMAGES

First, we identify a set of point sources as PSF/photometric references in the AFASS maps. Our aim here is to provide good-quality point sources that are reasonably bright in the far-IR. Thus, we opt to generate our own list of calibrators by selecting sources from the *AKARI* FIS Bright Source Catalog Ver. 2 (BSCv2; Yamamura et al. 2016) using the following two criteria: (1) FQUAL = 3 (the presence of the source is confirmed and its flux determined to be valid) in all four FIS bands, and (2) NDENS ≤ 2 (there are at most two nearby objects within $5'$ of the source). This initial filtering identifies 658 objects.

Next, we look at the AFASS maps at the coordinates of these 658 BSCv2 sources and measure the size of the full-width at half-maximum (FWHM) when there is a detection of an isolated emission peak at greater than 20 and $10\,\sigma$ in the wide (*WIDE-S* and *WIDE-L*) and narrow (*N60* and *N160*) bands, respectively. Then, we further eliminate sources by requiring that good PSFs are those that fall within the 95 % confidence interval of the mean FWHM size in the distribution of the FWHM size for these 658 sources. After this stringent filtering, we find 73, 78, 64, and 45 sources in the *N60*, *WIDE-S*, *WIDE-L*, and *N160* bands, respectively, as representative point sources. These sources turn out to be almost exclusively distant galaxies (about 88 %), and the rest is roughly equally split between stellar and unidentified objects, based on their SIMBAD designations[2].

Using the AFASS cutout images (of $20' \times 20'$) of the representative point sources as selected above, we compute the normalized median "super-PSF" image and the corresponding median absolute deviation (MAD) map for each FIS band (Figure 1). The MAD maps are made by taking the median of the absolute difference between each PSF image and the super-PSF image, and therefore, graphically indicate how individual PSF images are statistically different from the corresponding super-PSF image at each pixel.

The super-PSFs appear more elongated along the in-scan direction (i.e., along the ecliptic latitude) than along the cross-scan direction (i.e., along the ecliptic longitude), and more prominently in the SW than LW bands. The apparent elongation of these super-PSFs in the in-scan direction ($\sim 7'$; Figure 1) can be explained by smearing of bright point sources due to (1) the $3\rlap{.}'6\,\mathrm{s}^{-1}$ scan speed with a typical reset interval of 2 s, and (2) two possible scan directions (from N to S and S to N) depending on the time of observations. Overall, the PSF structure in the AFASS maps based on images of the BSCv2 point sources is consistent with that based on the Cohen standard stars (Arimatsu et al. 2014; Takita et al. 2015).

With the PSF shape established in each FIS band of the AFASS maps, we can determine the aperture correction factors based on the amount of encircled energy within a specific aperture defined by the relative surface brightness with respect to the peak intensity. Using the super-PSF profiles and their 2-D Gaussian fits, we calculate the divisible aperture correction factors as a function of the aperture size (Table 1).
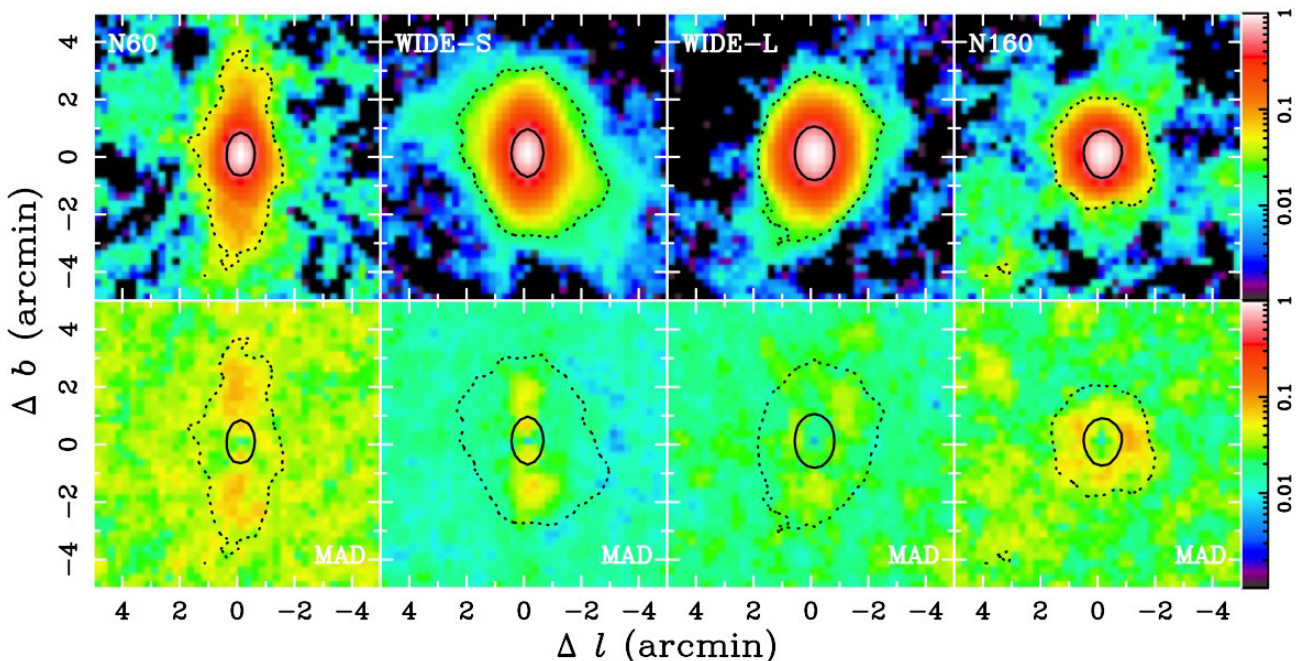

Figure 1. The *AKARI*/FIS super-PSF images (top row) and MAD maps (bottom row) in the *N60*, *WIDE-S*, *WIDE-L* and *N160* bands (top row; from left to right). The logarithmic color scaling of the images, from 0.1 % to 100 % relative to the peak intensity, is indicated in the wedge on the right. The solid and dotted contours represent the FWHM and $5\,\sigma$ detection level, respectively. The image orientation follows the ecliptic coordinates, which are adopted for the original AFASS maps.

---

[2] http://simbad.u-strasbg.fr/simbad/

Table 1. Aperture correction factors based on the super-PSFs

Aperture* (%)	N60	WIDE-S	WIDE-L	N160
90	0.071 ± 0.002	0.093 ± 0.001	0.084 ± 0.001	0.088 ± 0.001
80	0.208 ± 0.003	0.187 ± 0.003	0.176 ± 0.001	0.186 ± 0.002
70	0.258 ± 0.004	0.240 ± 0.003	0.301 ± 0.002	0.318 ± 0.003
60	0.311 ± 0.005	0.366 ± 0.004	0.406 ± 0.002	0.386 ± 0.004
50	0.426 ± 0.006	0.419 ± 0.005	0.463 ± 0.003	0.493 ± 0.005
40	0.497 ± 0.007	0.510 ± 0.005	0.559 ± 0.003	0.576 ± 0.007
30	0.546 ± 0.008	0.597 ± 0.006	0.646 ± 0.004	0.668 ± 0.008
20	0.652 ± 0.009	0.682 ± 0.007	0.751 ± 0.005	0.769 ± 0.010
10	0.737 ± 0.012	0.757 ± 0.008	0.853 ± 0.006	0.871 ± 0.012
8	0.766 ± 0.013	0.792 ± 0.008	0.861 ± 0.006	0.893 ± 0.013
5	0.800 ± 0.013	0.830 ± 0.008	0.911 ± 0.006	0.921 ± 0.014
1	0.895 ± 0.017	0.913 ± 0.009	0.978 ± 0.008	0.986 ± 0.015

*: The aperture size is defined by the percentage of the peak intensity.

3. PHOTOMETRY OF THE ADOPTED POINT SOURCES

3.1. Photometry with a 90″ radius aperture

First, we compare our photometry results using a fixed 90″ radius aperture against fluxes listed in BSCv2. The median of the uncorrected-AFASS-to-BSCv2 flux ratios in each band is found to be 0.67 ± 0.08, 0.70 ± 0.07, 0.68 ± 0.11, and 0.69 ± 0.19, for the *N60*, *WIDE-S*, *WIDE-L*, and *N160* bands, respectively. These values indicate that the 90″ radius aperture generally misses roughly 30% of the expected flux as previously found (Arimatsu et al. 2014; Takita et al. 2015). In fact, a fixed 90″ radius aperture of the super-PSFs translates to apertures defined by the surface brightness at 20 ± 9%, 27 ± 8%, 34 ± 8%, and 28 ± 7% of the peak intensity at *N60*, *WIDE-S*, *WIDE-L*, and *N160*, respectively. Each of these further translates to the aperture correction factor of 0.7 to 0.57 (Table 1). This is consistent with the median uncorrected-AFASS-to-BSCv2 flux ratio being about 68% across the bands. Hence, we confirm that the previously reported flux underestimates of about 30% were caused by the use of the fiducial 90″ aperture that missed the surface brightness component extending beyond the preset 90″ radius aperture.

3.2. Photometry with the derived aperture correction factors

Second, we compare our photometry results using the FWHM aperture (at 50% peak intensity) corrected for by the corresponding correction factors. With the aperture correction method, the corrected-AFASS-to-BSCv2 flux ratio is found to be 0.97 ± 0.14, 0.94 ± 0.10, 0.92 ± 0.10, and 0.82 ± 0.22. The derived ratio as a function of the BSCv2 flux for each band is shown in Figure 2. Here we confirm that the BSCv2 fluxes for the adopted point sources are reproduced within the margin of error, verifying the expectation that BSCv2 point-source fluxes can be recovered from the AFASS maps by PSF aperture photometry properly corrected for by aperture correction factors.

3.3. Photometry with the 1σ aperture without any correction

Third, we compare our photometry results using the 1σ aperture without any correction. This method practically corresponds to an infinite aperture for extended sources. We employ this method of photometry to verify the photometry results not only for point sources but also for extended sources. With this method, the AFASS-to-BSCv2 flux ratio is derived to be 1.31 ± 0.29, 1.11 ± 0.20, 1.05 ± 0.19, and 0.93 ± 0.21. The derived ratio as a function of the BSCv2 flux for each band is also shown in Figure 2. These measurements indicate that the BSCv2 fluxes are reproduced reasonably well with the photometry aperture set at the "edge" of the point sources at 1σ of the sky emission, albeit somewhat larger uncertainties. In genuinely extended sources, the distribution of surface brightness is supposedly not as centrally concentrated as in point sources, and hence, the flux overestimates seen above as a result of the source elongation would be expected to be less severe. Hence, we consider that the 1σ aperture method works reasonably well for any sources (point or extended alike, but preferably for extended sources for which the PSF aperture correction is not feasible).
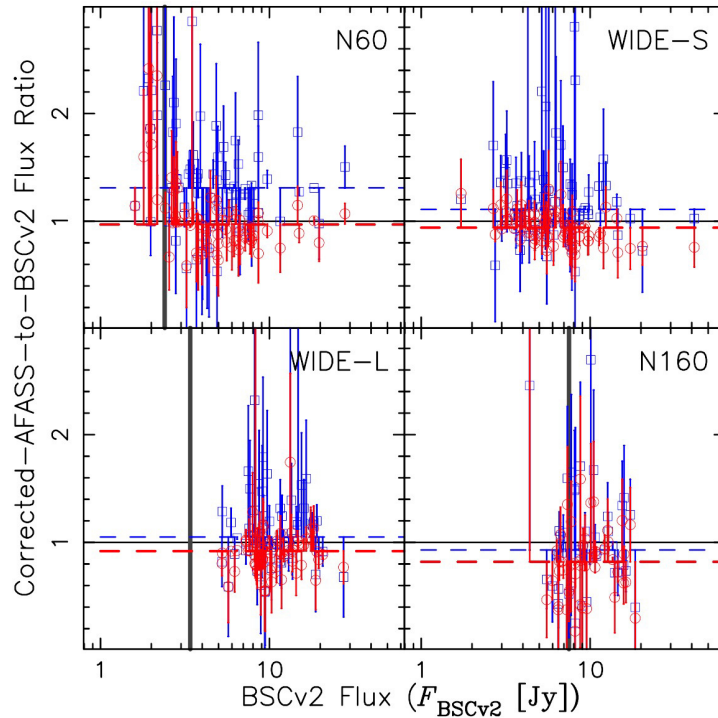
Figure 2. The corrected-AFASS-to-BSCv2 flux ratio vs. the BSCv2 flux for each FIS band as indicated. Red circles show the ratios based on the aperture correction method, while blue squares are those based on the $1\,\sigma$ aperture method. The black solid horizontal line shows the unity ratio, whereas the red and blue dashed lines indicate the median ratio for the aperture correction and $1\,\sigma$ aperture methods, respectively. The large scatters of the flux ratio are also previously reported by Takita et al. (2015) and was attributed to the difference in the actual photometry methods with the AFASS maps and in the BSC. The vertical thick gray lines indicate the BSCv2 detection limit at 2.4, 0.44, 3.4, and 7.5 Jy in the *N60*, *WIDE-S*, *WIDE-L*, and *N160* bands, respectively (Yamamura et al. 2016).

4. **FLUX CALIBRATIONS IN THE AFASS MAPS**

We verify that flux underestimates previously reported for point sources in the AFASS maps are caused by the adopted 90″ radius aperture, beyond which there still exists the fainter surface brightness component. For point sources, the total flux can be recovered by correcting the measured flux using the PSF aperture correction factor (Table 1). We confirm that the total flux of extended sources can also be recovered without any special correction by the use of an appropriate aperture that encompasses the entire extent of the target extended source. These findings suggest that the surface brightness of the AFASS maps is calibrated correctly for non-diffuse sources as well as diffuse sources. Therefore, AFASS map users can perform far-IR photometry for (1) point sources by using the PSF aperture correction method using the correction factors presented here (Table 1), and (2) extended sources by summing up surface brightnesses within an appropriate aperture of the target source and converting the pixel value sum into flux by multiplying by 5.29×10^{-3} ([Jy]/[MJy sr^{-1}]) $= 2.35 \times 10^{-5}$ ([Jy/sq. arcsec]/[MJy sr^{-1}]) $\times 15 \times 15$ (sq. arcsec). We are presently compiling fluxes of Galactic planetary nebulae detected in the AFASS maps to be presented elsewhere (Ueta et al. *in preparation*).

REFERENCES

Arimatsu, K., Doi, Y., Wada, T., et al. 2014, PASJ, 66, 47
Boggess, N. W., Mather, J. C., Weiss, R., et al. 1992, ApJ, 397, 420
Cohen, M., Walker, R. G., Carter, B., et al. 1999, AJ, 117, 1864
Doi, Y., Takita, S., Ootsubo, T., et al. 2015, PASJ, 67, 50
Gorjian, V., Wright, E. L., & Chary, R. R. 2000, ApJ, 536, 550
Hauser, M. G., Arendt, R. G., Kelsall, T., et al. 1998, ApJ, 508, 25
Kawada, M., Baba, H., Barthel, P., et al. 2007, PASJ, 59, S389
Matsuura, S., Shirahata, M., Kawada, M., et al. 2011, ApJ, 737, 2
Murakami, H., Baba, H., Barthel, P., et al. 2007, PASJ, 59, S369
Shirahata, M., Matsuura, S., Hasegawa, S., et al. 2009, PASJ, 61, 737
Takita, S., Doi, Y., Ootsubo, T., et al. 2015, PASJ, 67, 51
Ueta, T., Tomasino, R. L., Takita, S., et al. 2017, PASJ, 69, 11
Yamamura I., Makiuti S., & the AKARI team. 2016, AKARI-FIR Bright Source Catalogue Public Version 2, Release Note